Front. Earth Sci. 2017, 11(2): 416–426
DOI 10.1007/s11707-016-0591-2

RESEARCH ARTICLE

A geometric model of faulted detachment folding with pure shear and its application in the Tarim Basin, NW China

Zewei YAO[1], Guangyu HE (✉)[1], Xiaoli ZHENG[1], Chuanwan DONG[1], Zicheng CAO[2], Suju YANG[2], Yi GU[3]

1 School of Earth Sciences, Zhejiang University, Hangzhou 310027, China
2 SINOPEC Northwest Oilfield Company, Urumqi 830011, China
3 Wuxi Research Institute of Petroleum Geology, SINOPEC, Wuxi 214126, China

© Higher Education Press and Springer-Verlag Berlin Heidelberg 2016

Abstract We present an improved geometric model of faulted detachment folding with pure shear that is characterized by core thickening and a ramp-discordant backlimb. The model includes a two-stage evolution: 1) detachment folding involving pure shear with fixed hinges, and 2) faulted detachment folding, in which the core of anticline thrusts above a break-through fault in forelimb by limb rotation. The growth strata patterns of the model are also discussed with respect to factors such as limb rotation, tectonic uplift rate, and sedimentation rate. A thrust-related fold, called a TBE thrust fold, in the Tarim Basin in NW China, is analyzed as an example of the theoretical model. The result indicates that the TBE thrust fold has undergone a two-stage evolution with shortening of a few hundred meters. Both the theoretical model and the actual example indicate that the shortening in the detachment folding stage takes up a large proportion of the total shortening. The structural restoration of the TBE thrust fold also provides new evidence that the formation of a series of thin-skinned structures in the SE Tarim Basin initiated in the Late Ordovician. The model may be applicable to low-amplitude faulted detachment folds.

Keywords faulted detachment folding, geometric model, pure shear, growth strata, Tarim Basin, shortening

1 Introduction

Asymmetric thrust-related folds formed at fault-tips are an important structure style in many thrust belts, such as the Zagros thrust-fold belt, the Canadian Rockies, and the Utah-Wyoming-Idaho fold belt (Rowan, 1997; Mitra, 2002). Two classical kinematic models, including break-thrust folding and fault-propagation folding have been developed on the basis of the relative timing of folding and faulting to decipher the formation of these structures (Jamison, 1987; Mitra, 1990; Erslev and Mayborn, 1997). Break-thrust folds are formed when thrusts break through forelimbs of early buckle folds (Fig. 1(a)) (Fischer et al., 1992). In fault-propagation folds (Mitra, 1990; Suppe and Medwedeff, 1990; Tavani et al., 2006) (Figs. 1(b) and 1(d)), the faulting and folding are synchronous, transferring the fault slip to the fold amplification. This is supported by the fact that many asymmetry folds in thin-skinned thrust belts are only partially truncated by the faults (Erslev and Mayborn, 1997).

Recent detailed field observations and analog models of thrust belts indicate several more complicated kinematic mechanisms involving an initial stage of detachment folding followed by subsequent propagation of thrust faults (Storti and Poblet, 1997). Mitra (2002) classified this type of structure as a faulted detachment fold, and proposed an area-balance model for both symmetric and asymmetric faulted detachment folds (Fig. 1(c)). The model demonstrates the process that a fault propagates in deformation zones on the forelimb at a later stage of detachment folding, and finally the fault connects with the basal detachment to form a break-through fault.

Despite the variety of the kinematic and geometric solutions, available models of thrust-related folding do not yet account for the co-occurrence of some key features. These features are significant in the structural evolution of the fold. One observed example of a thrust fold found in seismic data includes the following two features: (i) the presence of the anticlinal backlimb panel that is not parallel to the thrust ramp, and (ii) the thickening of the core of the anticline. Based on these features, it is likely that the thrust fold is a faulted detachment fold with pure-shear strain. However, detailed geometric models of such structures are

Received July 22, 2015; accepted March 15, 2016

E-mail: hegy@zju.edu.cn

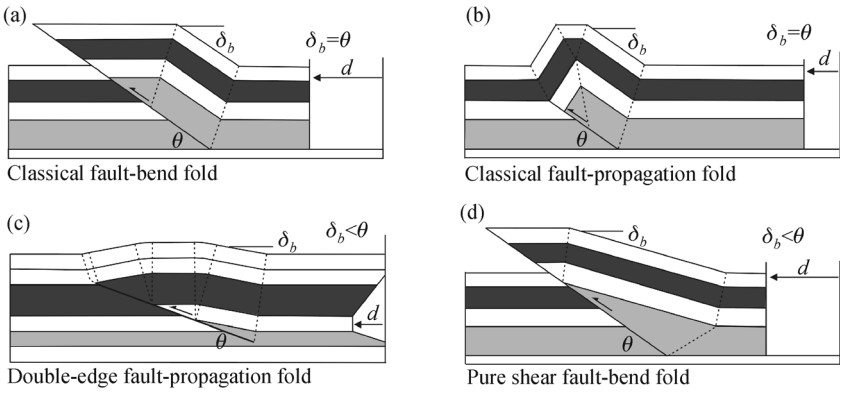

Fig. 1 Geometric models of four types of fault-related folding. (a) Break-thrust folding (modified from Fischer et al., 1992). (b) Classical fault-propagation folding (Suppe and Medwedeff, 1990). (c) Faulted detachment folding (Mitra, 2002). (d) Double-edge fault-propagation folding (Tavani et al., 2006). δ_b is backlimb dip and θ is ramp dip.

rarely described. Thus, modeling of these structures is of great significance in the present for further understanding of the deformation process.

In this paper, we propose an improved kinematic and geometric model called faulted detachment folding with pure shear which offers a possible evolution of fault-tip folds with the features mentioned above. In this model, a detachment fold is first formed through pure shear with fixed hinges (Groshong and Epard, 1994). Second, the detachment fold is faulted in the forelimb forming a break-through fold. The analytical solutions and the growth strata pattern of the model are also discussed. Finally, we apply the geometric model in a thrust-related fold in the Tarim Basin which is here called the TBE thrust fold.

2 Geometric model of faulted detachment folding with pure shear

2.1 Detachment folding

Conceptual models describing the geometries and kinematics of detachment folding have been proposed on the basis of mass-balance perspectives (Epard and Groshong, 1995; Homza and Wallace, 1995; Poblet et al., 1997; Mitra, 2002; Atkinson and Wallace, 2003; Mitra, 2003; Suppe, 2011). Field studies indicate that the dominant fold mechanism for these structures is limb rotation with constant limb length and a fixed hinge (Mercier et al., 2007). Based on these conditions, parallel folding with constant bed length requires a variable decollement depth, which is inconsistent with outcrop observations. One possible solution is that parallel strain (also called pure shear) exists in the fold.

Natural examples of detachment folding with pure shear are found in many regions, including the Yakeng anticline in the southern Tianshan thrust belt of western China, the Cascadia detachment fold of offshore Oregon, the Nankai detachment fold offshore of Japan (Gonzalez-Mieres and Suppe, 2006), and so on. These examples are characterized by low-amplitude detachment folds and composed of competent layers. Their shortening is dominantly accommodated by layer-parallel pure shear. These features suggest that pure shear can occur not only in the incompetent layers but also in competent layers, and it plays an important role in low-amplitude detachment folding.

As a result, the conceptual model of detachment folding proposed in this paper is deformed via pure shear (Groshong and Epard, 1994; Epard and Groshong, 1995) but with fixed hinges and rotating limbs (Fig. 2). During the detachment folding, the anticline is bounded by two fixed hinges with another inactive hinge fixing the core of the anticline (Figs. 2(a) and 2(b)). The strata within the anticline are deformed through pure shear and are thickened toward the hinge of the anticline. As a result, the strata within two fixed hinges suffer penetrative strain. The pure shear deformation of incompetent layers (basal detachment layers) differs from that of competent layers, as the competent layers control the main shape of the fold and the incompetent layers are deformed associated with competent layers. Although the incompetent layers may flow along the strike of the fold, it is assumed that their areas are constant in the two dimensional model for simplicity.

2.2 Faulted detachment folding

In the process of faulted detachment folding, the structural pattern in the conceptual model is controlled by two parallel and active hinges in additional to early axial surfaces formed during detachment folding (Fig. 2(c)). The kinematics are similar to shear fault-bend folding (Suppe et al., 2004). One axial surface is developed in the cutoff point of bottom competent layers in the hanging wall. The other is close to the hinge of the syncline, which is

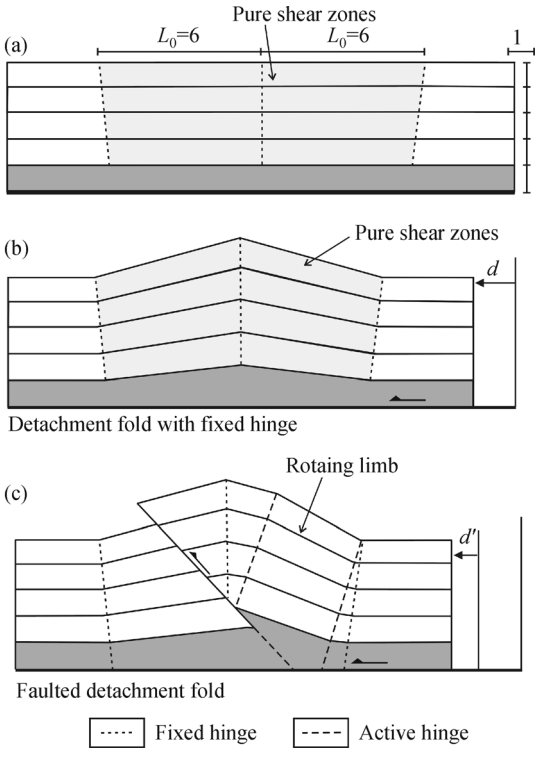

Fig. 2 Stepwise evolution of faulted detachment folding with pure shear. (a) Initial geometry of faulted detachment fold, where initial limb length L_0 is approximately 6 units and the thickness of layer is 1 unit. (b) Fixed-hinge, low-amplitude, symmetric detachment fold formed with pure shear (modified from Epard and Groshong, 1995). (c) Break-through folding with a fault in forelimb of detachment fold with increased shortening. The strata of grey in the base are the basal detachment layers.

generally fixed relative to the rock layers. This is because we find it intuitively likely that the axial surface is easily formed near the core of syncline. With increasing shortening, the dip of the backlimb increases and strata in the core of the anticline are uplifted with constant dip and thickness, resulting in the same displacements of different layers.

2.3 Growth strata in faulted detachment folding

Growth strata are regarded as a useful tool to study the kinematics of thrust folds (Suppe et al., 1997; Salvini and Storti, 2002) because in some cases, structures with different evolution paths may have analogous final structural shapes. Several factors such as limb rotation, limb length widening, tectonic uplift rates, sedimentation rates, and erosion rates influence growth stratal architectures (Poblet et al., 1997; Storti and Poblet, 1997). Here we carry out forward modeling of growth strata of the faulted detachment fold using a semi-quantitative approach based on a velocity model.

The velocity model of progressive limb rotation was first proposed by Hardy and Poblet (1994) to observe the pattern of growth strata on the rotating limb with a constant limb length and shortening rate. The growth strata progressively onlap the dipping limb, and eventually overlap the crest when the shorten rate and sedimentation rate is constant (Fig. 3) (Hardy and Poblet, 1994). This is because under this condition the rate of limb rotation and limb uplift decreases with increasing shortening (Figs. 4(a) and 4(b)).

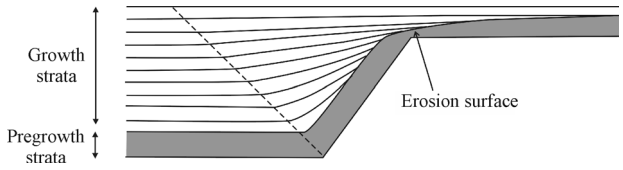

Fig. 3 Numerical model of growth sedimentation and progressive limb rotation (Hardy and Poblet, 1994).

The results suggest that the relative rates of limb rotation and uplift directly control the pattern of the growth strata. Thus we analyzed the characteristics of limb rotation and uplift of faulted detachment folding with pure shear under the condition of constant shortening rate to present the growth strata patterns. As the conceptual model is composed of a two-stage evolution, the results are proposed sequentially. The model is based on the given condition presented in Fig. 2(a) where the ratio of limb length to total layer thickness is 6:5. Though it only represents one case of the detachment folds with pure shear, it reflects the main features. Growth strata patterns are proposed in two cases: when the uplift rate is larger or smaller than the sedimentation rate.

In the detachment folding stage, the limb rotation rate slightly decreases and then slightly increases with continued shortening (Fig. 4(c)). The transition occurs at a point when shortening is approximately 3 units. The limb uplift rate slightly increases with increasing shortening, and the limb length is shortened and then lengthened (Fig. 4(d)). This occurs at a point where shortening is between 2 and 3 units. We only discuss the detachment fold with low amplitude where the total shortening is less than 3 units. Therefore, the deformation of the anticline limb is approximated by limb rotation with constant limb length and constant uplift rate. The effects of pure shear on the overlying growth strata are also neglected. This is because the growth strata are unconsolidated.

Thus growth strata may exhibit a fan pattern on the limbs of the anticline in the detachment folding stage in both cases, when the uplift rate is larger or smaller than the sedimentation rate (Figs. 5(a) and 5(c)). The effects of erosion, redeposition, and compaction of syntectonic sedimentation are also neglected in this work.

During the sedimentation of the break-through stage of fault detachment folding, the growth strata have a shape similar to the progressive limb rotation model (Fig. 3). The

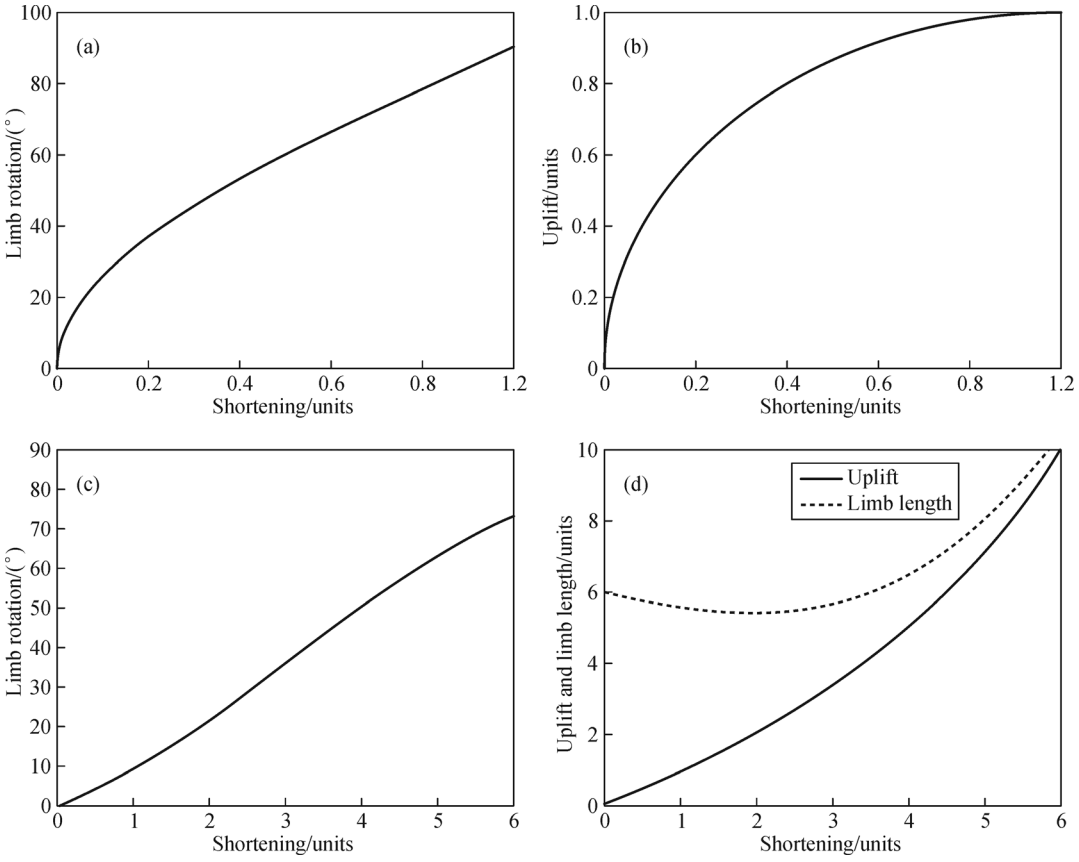

Fig. 4 Relations of limb rotation (a), (c) and uplift (b), (d) and limb length (d) versus shortening for different models. (a), (b) corresponding to the model of progressive limb rotation (Hardy and Poblet, 1994). (c), (d) corresponding to the detachment fold under given conditions (see text for detail). The shortening unit in (a), (b) is the limb length and in (c), (d) is the thickness of single layer.

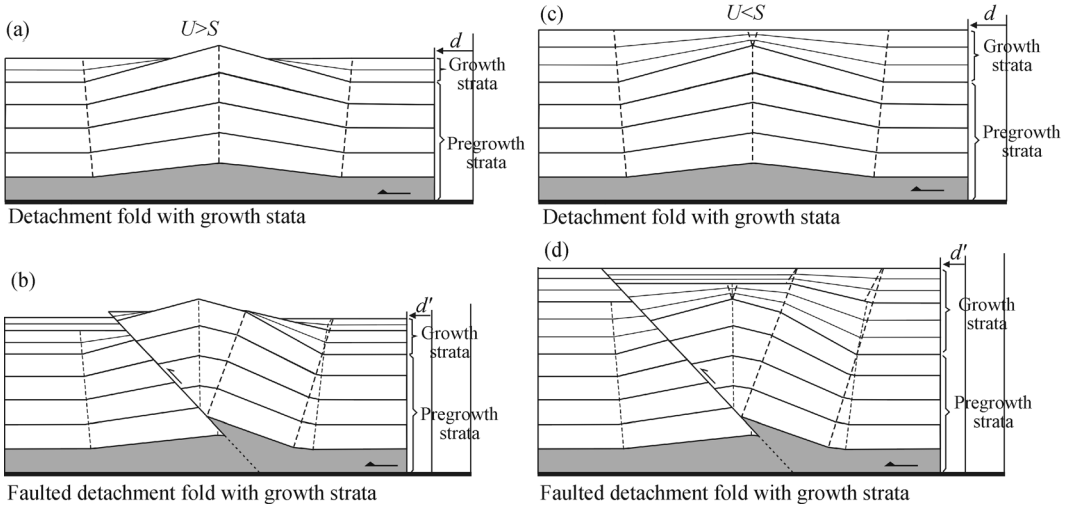

Fig. 5 Forward modeling of growth faulted detachment folding with certain simplifications for uplift rate larger than sedimentation rate (a), (b) and for uplift rate less than sedimentation rate (c), (d). U = uplift rate, S = sedimentation rate. Note the growth strata at detachment folding stage are thicker than that at break-through stage.

backlimb, bounded by two active axial surfaces, rotates with the increasing shortening, but the uplift rate decreases rapidly as the shortening accumulates. Thus the growth strata may overlap the backlimb when the uplift rate is

larger than the sedimentation rate (Fig. 5(b)). The growth strata would cover the crest of the fold when the sedimentation rate is larger than the uplift rate (Fig. 5(d)).

2.4 Analytical solutions of faulted detachment folding

2.4.1 Detachment folding

The main purpose for a quantitative description of faulted detachment folding is to obtain the shortening from thrusting. Although an algorithm describing shortening during detachment fold has already been discussed in a number of published works (Gonzalez-Mieres and Suppe, 2006; Hubert-Ferrari et al., 2007; Ramon and Suppe, 2011; Suppe, 2011), some relationships need more discussion.

The shortening of detachment fold can be obtained from the area-balance theory in two dimensional systems. This means that shortening area is equal to the area of folded layer above its undeformed horizon (Fig. 6) which can be expressed as $hS = A_b$. The total shortening S is $2(L_0 - L\cos\theta)$, where L_0 is the initial limb length and L is the current limb length. The difference between L_0 and L is used to obtain the magnitude of pure shear shortening S_ε as $S_e = 2(L_0 - L)$. The difference between S and S_ε is $L(1-\cos\theta)$, called the bed-length shortening.

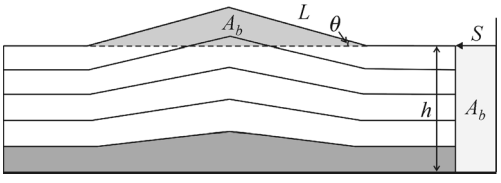

Fig. 6 A detachment fold showing contrasting measures of shortening. The initial limb length is L_0. S is horizontal shortening. A_b is the area of the triangle with grey color (modified from Suppe, 2011)

Based on these mathematical relationships and the prescribed conditions in Fig. 2(a), we can obtain the component of S_ε in the total shortening with the specific relation between L_0 and h (Fig. 7). That figure illustrates that the component of pure shear shortening in the upper section (relatively large h) is larger than that in the lower section (relatively small h) with the same horizontal shortening, and that the bed-length shortening is much smaller than the pure-shear shortening at low limb dips ($< 10°$). This means that the pure shear shortening accommodates most of shortening at low limb dips.

2.4.2 Faulted detachment folding

The derivation of the equations describing the shortening of a faulted detachment fold including parameters of displacement, backlimb dip, and shortening are based on the model below (Fig. 8):

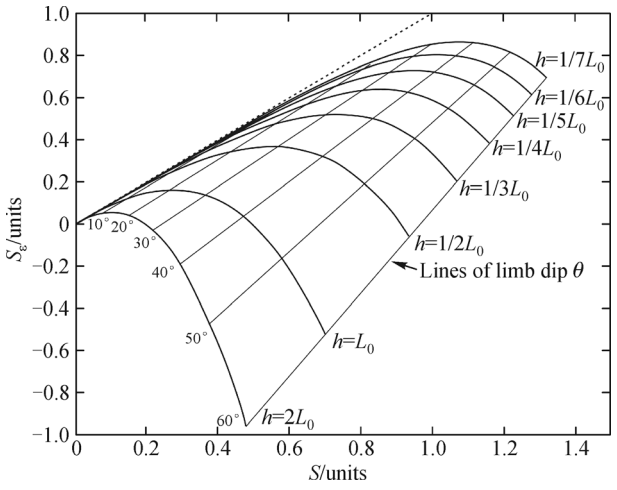

Fig. 7 Relations of total shortening and pure shear shortening in detachment fold with pure shear in the case where $\theta <= 60°$. The distance between curve and dotted line is the bed-length shortening. The unit of S and S_ε is the undeformed limb length L_0.

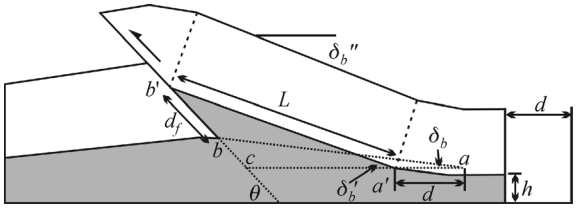

Fig. 8 Geometric elements used in the derivation of relationships of shortening, uplift, and displacement. See text for detail.

In the evolution of the faulted detachment fold, the ramp dip θ remains constant, the position of backlimb migrates from ab to $a'b'$ with constant limb length L, and the backlimb dip changes from δ_b to δ_b'. We set $L = 1$ unit. In the triangle abc and $a'b'c'$ by the law of sines we obtain:

$$\frac{bc}{\sin\delta_b} = \frac{L}{\sin\theta} = \frac{b'c}{\sin\delta_b'}, \tag{1}$$

From Eq. (1) we can obtain the equation for fault displacement d_f:

$$d_f = b'c - bc = L(\sin\delta_b'/\sin\theta - \sin\delta_b/\sin\theta). \tag{2}$$

Similarly, we obtain the ratio of horizontal slip d (shortening):

$$d = ca - ca' = L[\sin(\theta-\delta_b)/\sin\theta - \sin(\theta-\delta_b')/\sin\theta]. \tag{3}$$

Eqs. (2) and (3) indicate that d_f and d are the difference of function of δ_b in a given structure, where L and θ remain constant during deformation. We draw the function of $\sin\delta_b/\sin\theta$ and $\sin(\theta-\delta_b)/\sin\theta$ (Fig. 9). We can obtain the horizontal slip d by the difference of function of $\sin\delta_b/\sin\theta$ and $\sin(\theta-\delta_b)/\sin\theta$ with changed dip δ_b along the curve of certain ramp dip θ. As in the example of the TBE thrust

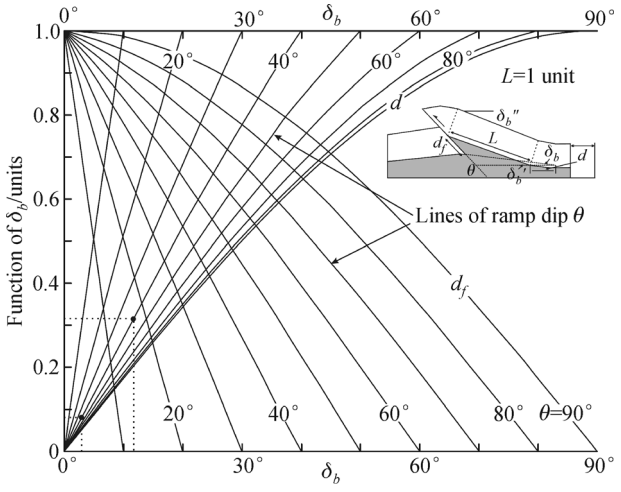

Fig. 9 Graph of relationships between shortening d and displacement d_f verse backlimb dip δ_b with certain ramp dip θ based on Eqs. (2) and (3).

fold, θ and L are 40° and 1.8 km, respectively, and δ_b changes from 2° to 12°. The difference of function of δ_b with d is approximately 0.27, which multiplied by L is approximately 480 m. So the horizontal shortening d is approximately 480 m.

3 An example from the Tarim Basin

A good example of a faulted detachment fold, called the TBE thrust fold, is imaged in seismic data from the Tanggubasi depression of the Tarim Basin.

3.1 Generalized structure and stratigraphy

The Tarim Basin is a large oil-bearing basin in northwestern China. Multi-phased tectonic events from the Cambrian through the Cenozoic have led to the development of a series of paleo-uplifts and depressions of different ages within the basin (Lin et al., 2012).

The Tanggubasi depression is a pre-Silurian sub-basin located in the Central uplift of the Tarim Basin (Fig. 10). The depression is strongly asymmetric. It is bounded by the Zhong2 fault to the north and the Cheerchen fault to the southeast. To the southwest, the southwest flank dips gently to the Magaiti slope.

Cambrian to Middle Ordovician strata in the Tanggubasi depression were deposited on flat-lying pre-Cambrian basement (Fig. 11). Major units include the Xiaoerbulaike, Wusongeer, Awatage, Qiulitage, Penglaiba, Yinshan, and Yijianfang formations, which are mainly composed of marine deposits including dolomite, micrite, and gypsum. Gypsumis mainly developed in the Middle and Lower Cambrian, acting as an important regional detachment layer. When deposition ended in the Middle Ordovician, the Tarim Basin suffered deformation from the Kunlun orogeny. The dominant direction of compression in the study area was SSW−NNE, which led to the initial uplift of the NWW−SEE-trending Tazhong uplift. As a result, the Yijianfang formation through most of the Tazhong uplift was eroded (Cai and Li, 2008). The contrast in structural relief between the Tanggubasi depression and the Tazhong uplift began to form.

During the deposition of Qiaerbake, Lianglitage, and lower Sangtamu formations, the Tazhong uplift continued to rise, resulting in the overlapping of Upper Ordovician units from the Tanggubasi depression on the Tazhong uplift (Fig. 11). Reefs and limestones were developed along the margins of the Tazhong uplift. During the end of the Ordovician, thrusting from the Kunlun and Altun orogenies led to the formation of a series of NE-trending thin-skinned thrust-related fold belts in the southeastern part of the Tarim Basin (He et al., 2011; Ren et al., 2011; Xu et al., 2011). Recent discovery of growth strata of the

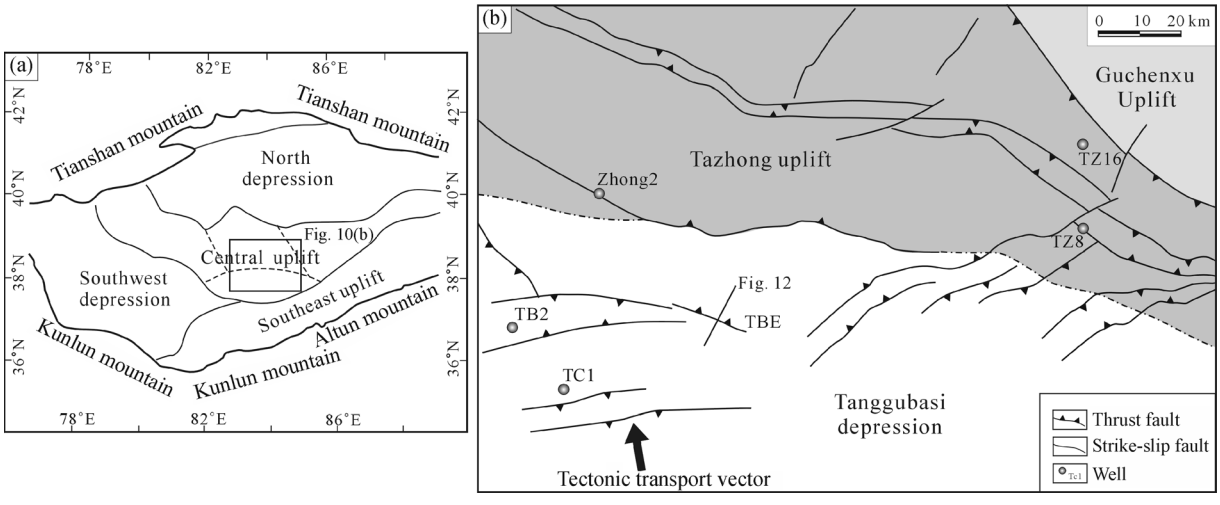

Fig. 10 (a) Sketch map of tectonic units of the Tarim Basin. (b) Location of the TBE thrust fold in the Tanggubasi depression of the Central uplift of the Tarim Basin.

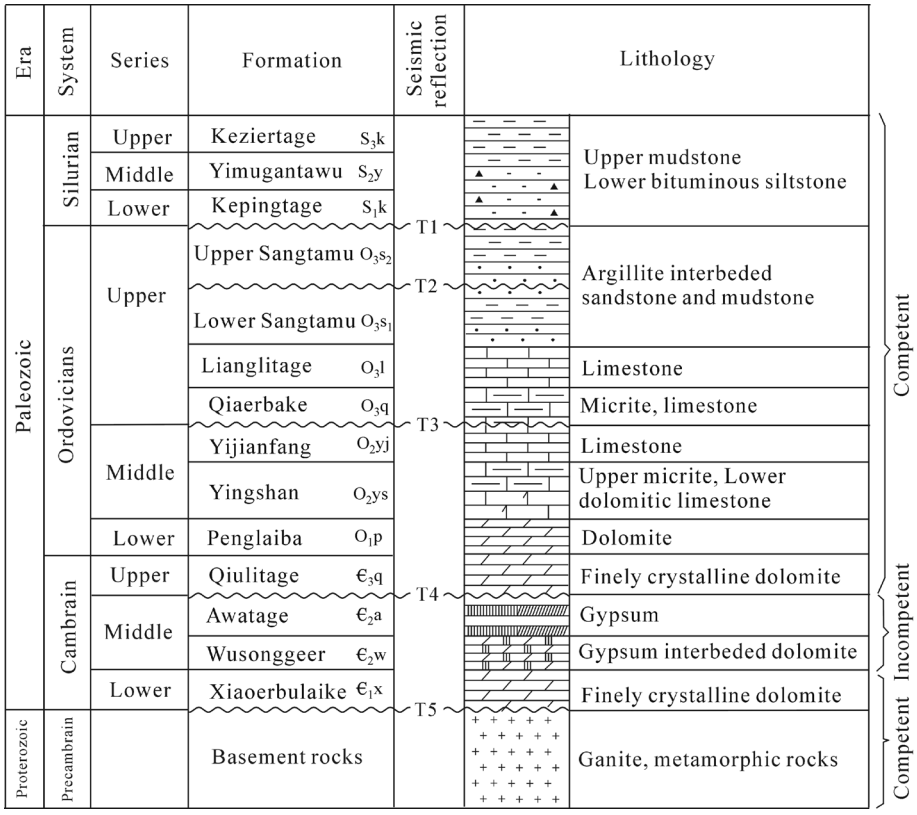

Fig. 11 A schematic diagram showing stratigraphic units in the Tanggubasi depression, Tarim Basin.

Sangtamu formation indicates that these NE-trending faults started to form in the Late Ordovician (Li et al., 2013). At the end of the Ordovician, the Central uplift of the Tarim Basin experienced tectonic uplift resulting in a large amount of erosion of the Upper Ordovician strata. Some hundreds of meters of Silurian rocks were deposited gently on the Tanggubasi depression and adjacent area with somewhat uniform thickness.

The thin-skinned thrust faults in the NW corner of the Tanggubasi depression slightly changed their trends from NE to NEE or EW. Thus the tectonic transport vector was NNW (Fig. 10(b)). The TBE thrust-related fold is one of these faults. It has not been systematically studied and named, so we temporally name it as TBE thrust fold as it locates in the east of the TB2 well (Fig. 10(b)). In the eastern part of the Tanggubasi depression, a series of the NE-trending faults formed. These folds were initially formed in the end of the Ordovician and superimposed with oblique slips during the Silurian and Devonian (Ren et al., 2011).

3.2 The TBE thrust fold

Though the TBE thrust fold does not trend perpendicular to the main tectonic transport vector, which may lead to the oblique slip, there is no significant slip observed in the cross-section of the structure. As a result, we ignore possible oblique slip in the TBE thrust fold in the following discussion.

The TBE thrust fold is imaged by a high-quality seismic survey, and the trend of seismic profile used in this paper is perpendicular to the fold hinge (Figs. 10 and 12(a)). A time to depth conversion is made on the hypothesis that velocity is a function of the stratigraphic layers (i.e., constant interval velocities). Velocities of strata used in conversion are derived from adjacent well TC1 (Tacan1) (Fig. 10).

In cross-section, the TBE thrust fold is characterized as an asymmetric anticline cut by a fault which originates in an incompetent layer (Fig. 12). The fault is SSW-vergent and the folded strata include Upper Cambrian units to the lower Sangtamu formation of the Upper Ordovician strata, which are overlain by the upper Sangtamu formation. On the top of the upper Sangtamu formation, there is Silurian strata which gently cover the structure.

Evaporites, including gypsum in the Middle and Lower Cambrian, compose the basal detachment layer which is thickened in the core of the anticline and thinned towards the core of syncline. This indicates the flow of the incompetent layer from the core of syncline to the core of anticline. A normal fault is developed below the reverse fault, with a thickened hanging wall consisting of middle and lower Cambrian indicating that it was formed during the deposition of Middle and Lower Cambrian.

It is clear that the structure is a thrust-related fold, but

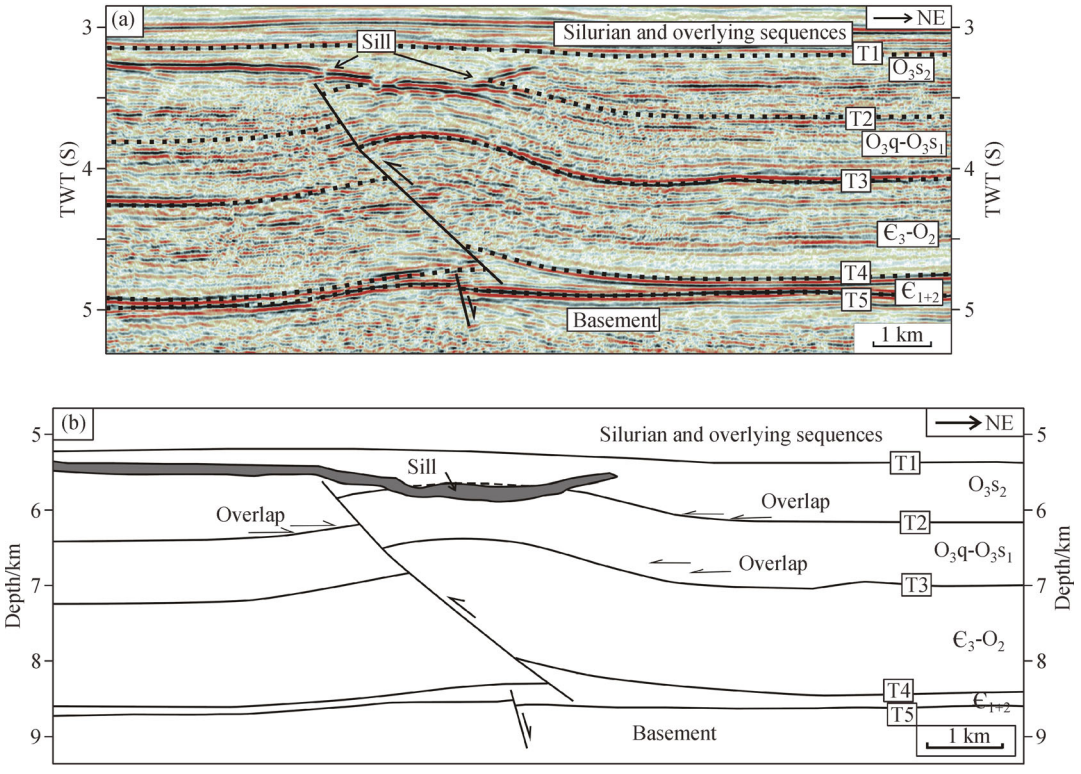

Fig. 12 (a) Interpreted seismic profile of TBE thrust fold (for location see Fig. 10). Vertical exaggeration is approximately 1. (b) Line drawings of time-depth converted seismic profile of the TBE thrust fold. The seismic reflection interfaces T1, T2, T3, T4, T5 are the stratigraphic boundaries of certain units (see Fig. 11 for detail). TWT: two-way travel time.

further characterization is complicated. One reasonable explanation, suggested by some key features, is that it is dominantly a faulted detachment fold with pure shear:

1) The footwall is also bent with basal detachment units accumulated in the core of anticline. This demonstrates an initial detachment folding stage in the deformation history.

2) The backlimb of the anticline of the hanging wall dips more gently than the fault plane. Anticlinal backlimbs that dip parallel to the thrust ramps are deformed by shear fault bend folding (Suppe et al., 2004), double-edge fault-propagation folding (Tavani et al., 2006), and faulted detachment folding (Mitra, 2002) (Fig. 1). As the example can therefore not be classified as either of the two previous ones, it is most likely a faulted detachment fold.

3) The dips of the hanging wall beds and footwall beds are nearly the same, and the displacements decrease very slightly along the fault (Fig. 13). This indicates that the fault formed subsequent to the folding without significant transfer of fault slip to the fold amplitude.

4) Upper Cambrian to Middle Ordovician units in the core of the anticline in the hanging wall and the north limb of the syncline of the footwall are thickened (Fig. 12).

Thus we propose that the TBE thrust fold is a faulted detachment fold with pure shear. As derived from the theoretical model, it commenced as a detachment fold with pure shear and later was deformed by break-through faulting in its forelimb.

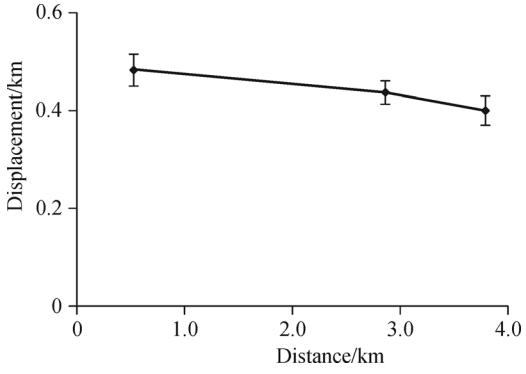

Fig. 13 Displacement–distance diagram showing that displacement decreases slightly with increasing distance. The three dots from left to right correspond to T4, T3, and T2, respectively. The decrease of displacement may be due to drag effect of the reverse fault.

3.3 Structural restoration

The structure is restored in two stages including break-through stage and detachment folding stage. In break-through stage, as mentioned in section 2.4.2, the shortening is approximately 480 m based on the model in Fig. 5 and Fig. 8, as the limb length is approximately 1.8 km.

In the detachment folding stage the shortening is calculated for every layer. As mention above, total shortening is composed of bed-length shortening and pure shear shortening. The total shortening can be calculated by thickness-relief methods based on a mass balance perspective (Gonzalez-Mieres and Suppe, 2006; Hubert-Ferrari et al., 2007). Measurements area of relief as a function of height can be plotted, and the local slope of the data is the total shortening (Fig. 14). The bed-length shortening can be calculated by measurement. Thus the pure shear shortening is the difference between total shortening and bed-length shortening.

The results show that total shortening of three layers are inconsistent (Fig. 14). The area of structural relief of T4 is relatively large. This may be caused by the flow of ductile units from the syncline to the anticline, which leads to the calculated total shortening of T4 being much larger that of T3 and T2. The structural relief of T2 is small. As a result, the calculated total shortening of T2 is close to 0. The most likely explanation is that strata bounded by T2 and T3 are growth strata. This is supported by some obscure onlap strata in the backlimb of the Lianglitage formation and Lower Sangtamu formation (Fig. 12). This indicates that the structure formed in the Late Ordovician (Fig. 15), which is consistent with observations in the Madong thrust belts (Li et al., 2013) located in the southwest of the TBE thrust fold as the southern part of the NE-striking thrust-related folds. Thus the shortening of T3 is the most reliable value at approximately 950 m. The results also indicate that the values of bed length shortening are one or two magnitude smaller than pure shear shortening (Fig. 14(b)), indicating the pure shear is the dominant mechanism (Fig. 7).

4 Discussion

Detachment folds show diverse geometries and deformation histories as a result of differences in mechanical stratigraphy, relative thickness of incompetent and competent layers, and diversity in tectonic events. In particular, a detachment fold with thick competent units and thin ductile units may form a low-amplitude fold followed by a fault truncating its forelimb due to the insufficiency of mobile detachment units to supply the volume required by the fold core (Stewart, 1996).

It is observed that pure shear deformation has a large impact on many low-amplitude detachment folds (Suppe, 2011). In these examples, pure shear deformation accommodates most of the shortening (Suppe, 2011), as observed in the TBE thrust fold. It is possible that pure shear shortening is also significant in many large-amplitude detachment folds. However, the shortening mechanism in these folds could be more complicated than that in low-amplitude folds, including secondary folding and/or subordinate synthetic and antithetic faulting.

Thus, the model presented in this paper may only be applicable to low-amplitude faulted detachment folds with a relative thin detachment unit. The low-amplitude faulted detachment fold is not a rigid concept. In this paper, a low-amplitude faulted detachment is roughly defined as having shortening less than 2 units in the detachment folding stage and 1unit in the faulted detachment folding stage. In other words, the shortening is less than c.25% and the backlimb dips less than 40°.

The deformation history of the TBE thrust fold has at least two geological implications. First, it should be noted that the shortening in the detachment folding stage is larger than that in the faulted detachment fold, although the former is not apparent in the seismic profile. This may be because the shortening is mostly accommodated by pure shear and expressed as slight thickening of the layer towards the hinge of the anticline. Moreover, the structural restoration of the TBE thrust fold also provides new evidence that the formation of a series of thin-skinned structures in the SE Tarim Basin began in the Late Ordovician.

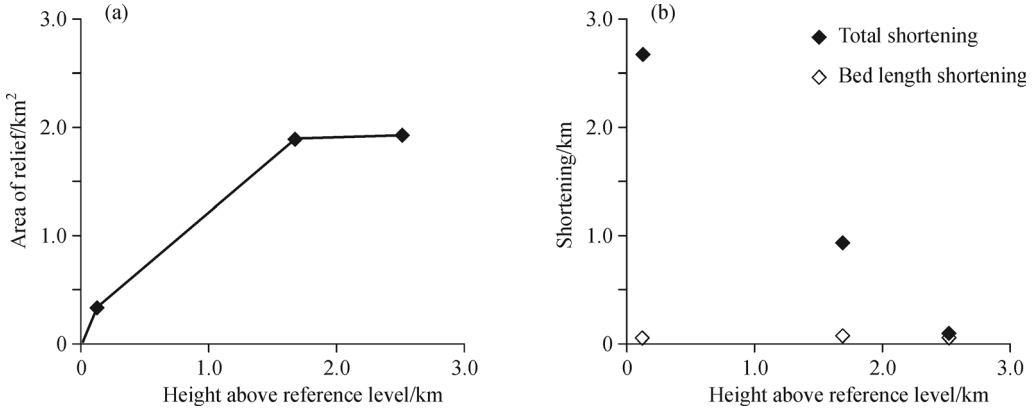

Fig. 14 (a) Areas of relief are plotted versus height above reference level and the slope is the total shortening. (b) Bed length shortening and total shortening. Note that reference level is the base of Cambrian. Three points is the shortening of T4, T3, and T2, respectively.

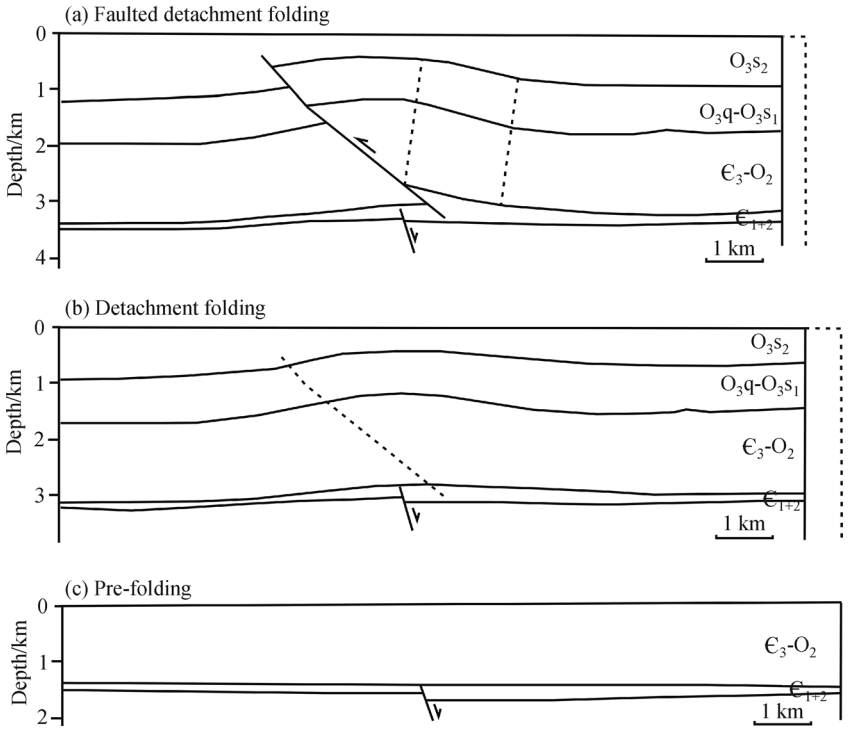

Fig. 15 Restoration cross-sections of the TBE thrust fold. (a) Faulted detachment folding during deposition of upper Sangtamu formation. (b) Detachment folding during deposition of the Qiaerbake formation to the Sangtamu formation. (c) Pre-folding stage at the end of the Middle Ordovician.

5 Conclusions

In this paper, we propose a geometric model of faulted detachment folding with pure shear, which is characterized by core thickening and a backlimb panel not dipping parallel to the ramp. The model includes a two-stage evolution: 1) detachment folding involving pure shear deformation of competent layers and flow of ductile layers with fixed hinges, and 2) faulted detachment folding, in which the backlimb is thrust above a break-through fault in the forelimb by limb rotation.

Forward modeling also describes the growth strata pattern with consideration of several factors, such as limb rotation, tectonic uplift rate, and sedimentation rate. Two scenarios are proposed: 1) a constant sedimentation rate lower than the uplift rate, and 2) a constant high sedimentation rate higher than uplift rate.

The TBE thrust fold from the Tarim Basin in NW China is studied as an example of the faulted detachment fold. The results indicate that the TBE thrust fold has undergone a two-stage evolution with a shortening of several hundred meters. Both the theoretical model and the actual example indicate that the shortening in the detachment folding stage takes up a large proportion of the total shortening in faulted detachment folding. The structural restoration of the TBE thrust fold also provides new evidence that the Late Ordovician is the initial time of the formation of a series of thin-skinned structure in the SE Tarim Basin.

Acknowledgements We wish to thank Chenxi Jiang in the Zhejiang University for her helpful support. Three anonymous reviewers are thanked for their thorough reviews and constructive comments, which greatly improved the article.

References

Atkinson P K, Wallace W K (2003). Competent unit thickness variation in detachment folds in the Northeastern Brooks Range, Alaska: geometric analysis and a conceptual model. Journal of Structural Geology, 25(10): 1751–1771

Cai X Y, Li Y (2008). Ordovician lithofacies and stratigraphic lacunae in the southern part of the Central Tarim, Xinjiang. Journal of Stratigraphy, 32(4): 353–362 (in Chinese)

Epard J L, Groshong R H Jr (1995). Kinematic model of detachment folding including limb rotation, fixed hinges and layer-parallel strain. Tectonophysics, 247(1−4): 85–103

Erslev E A, Mayborn K R (1997). Multiple geometries and modes of fault-propagation folding in the Canadian thrust belt. Journal of Structural Geology, 19(3−4): 321–335

Fischer M P, Woodward N B, Mitchell M M (1992). The kinematics of break-thrust folds. J Struct Geol, 14(4): 451–460

Gonzalez-Mieres R, Suppe J (2006). Relief and shortening in detachment folds. Journal of Structural Geology, 28(10): 1785–1807

Groshong R H, Epard J J (1994). The role of strain in area-constant detachment folding. Journal of Structural Geology, 16(5): 613–618

Hardy S, Poblet J (1994). Geometric and numerical model of progressive

limb rotation in detachment folds. Geology, 22(4): 371–374

He B Z, Jiao C L, Xu Z Q, Cai Z Q, Liu S L, Zhang Y L (2011). Manifestation of the Middle-Late Caledonian tectonic movement along the Altun-West Kunlun orogenic belt in the Tangguzibas depression, Tarim Basin. Yanshi Xuebao, 27(11): 3435–3448 (in Chinese)

Homza T X, Wallace W K (1995). Geometric and kinematic models for detachment folds with fixed and variable detachment depths. J Struct Geol, 17(4): 575–588

Hubert-Ferrari A, Suppe J, Gonzalez-Mieres R, Wang X (2007). Mechanisms of active folding of the landscape (southern Tian Shan, China). Journal of Geophysical Research-Solid Earth, 112(B3): 485–493

Jamison W R (1987). Geometric analysis of fold development in overthrust terranes. Journal of Structural Geology, 9(2): 207–219

Li H W, Wu G H, Shi L L, Wang B, Gao L (2013). The structural features and evolution series of Madong thrust belt, west of Tarim Basin. Xingjiang Geology, 31(3): 180–185 (in Chinese)

Lin C, Yang H, Liu J, Rui Z, Cai Z, Zhu Y (2012). Distribution and erosion of the Paleozoic tectonic unconformities in the Tarim Basin, Northwest China: significance for the evolution of paleo-uplifts and tectonic geography during deformation. J Asian Earth Sci, 46(2): 1–19

Mercier E, Rafini S, Ahmadi R (2007). Folds kinematics in “Fold-and-Thrust Belts” the “hinge migration” question, a review. In: Lacombe O, LavéJ, Roure F, Vergés J, eds. Thrust Belts and Foreland Basins: From Fold Kinematics to Hydrocarbon Systems. Berlin: Springer, 135–147

Mitra S (1990). Fault-propagation folds geometry, kinematic evolution, and hydrocarbon traps. AAPG Bull, 74(6): 921–945

Mitra S (2002). Structural models of faulted detachment folds. AAPG Bull, 86(9): 1673–1694

Mitra S (2003). A unified kinematic model for the evolution of detachment folds. Journal of Structural Geology, 25(10): 1659–1673

Poblet J, McClay K, Storti F, Munoz J A (1997). Geometries of syntectonic sediments associated with single-layer detachment folds. J Struct Geol, 19(3−4): 369–381

Ramon G, Suppe J (2011). Shortening histories in active detachment folds based on area-of-relief methods. In: McClay K, Shaw J, Suppe J, eds. Thrust Fault-Related Folding, AAPG Memoir 94. Tulsa: AAPG, 39–67

Ren J Y, Zhang J X, Yang H Z, Hu D S, Li M, Zhang Y P (2011). Analysis of fault systems in the Central uplift, Tarim Basin. Yanshi Xuebao, 27(1): 219–230 (in Chinese)

Rowan M G (1997). Three-dimensional geometry and evolution of a segmented detachment fold, Mississippi Fan foldbelt, Gulf of Mexico. J Struct Geol, 19(3−4): 463–480

Salvini F, Storti F (2002). Three-dimensional architecture of growth strata associated to fault-bend, fault-propagation, and décollement anticlines in non-erosional environments. Sediment Geol, 146(1–2): 57–73

Stewart S A (1996). Influence of detachment layer thickness on style of thin-skinned shortening. Journal of Structural Geology, 18(10): 1271–1274

Storti F, Poblet J (1997). Growth stratal architectures associated to decollement folds and fault-propagation folds. Inferences on fold kinematics. Tectonophysics, 282(1–4): 353–373

Suppe J (2011). Mass balance and thrusting in detachment folds. In: McClay K, Shaw J, Suppe J, eds. Thrust Fault-Related Folding, AAPG Memoir 94. Tulsa: AAPG, 21–37

Suppe J, Connors C D, Zhang Y (2004). Shear fault-bend folding. In: McClay K R, ed. Thrust Tectonics and Hydrocarbon Systems, AAPG Memoir 82. Tulsa: AAPG, 303–323

Suppe J, Medwedeff D A (1990). Geometry and kinematics of fault-propagation folding. Eclogae Geol Helv, 83(3): 409–454

Suppe J, Sabat F, Munoz J A, Poblet J, Roca E, Verges J (1997). Bed-by-bed fold growth by kink-band migration: Sant Llorenc de Morunys, eastern Pyrenees. Journal of Structural Geology, 19(3−4): 443–461

Tavani S, Storti F, Salvini F (2006). Double-edge fault-propagation folding: geometry and kinematics. Journal of Structural Geology, 28 (1): 19–35

Xu Z Q, Li S T, Zhang J X, Yang J S, He B Z, Li H B, Lin C S, Cai Z H (2011). Paleo-Asian and Tethyan tectonic systems with docking the Tarim block. Yanshi Xuebao, 27(1): 1–22 (in Chinese)